frontiers in Marine Science

ORIGINAL RESEARCH
published: 28 September 2021
doi: 10.3389/fmars.2021.732720

Mercury Accumulation in Marine Sediments – A Comparison of an Upwelling Area and Two Large River Mouths

Sara Zaferani and Harald Biester*

Institute for Geoecology, Environmental Geochemistry Group, Technische Universitaet Braunschweig, Braunschweig, Germany

Understanding marine mercury (Hg) biogeochemistry is crucial, as the consumption of Hg-enriched ocean fish is the most important pathway of Hg uptake in humans. Although ocean sediments are seen as the ultimate Hg sink, marine sediment studies on Hg accumulation are still rare. In this context, studying Hg behavior in the marine environment, especially in upwelling environments, is of particular interest due to its importance in these great upwelling regions for the global fishery. There are contradictory statements about the fate of Hg in upwelling regions. Some studies have suggested high biotic reduction of oxidized Hg and gaseous elemental mercury evasion to the atmosphere. More recent work has suggested that in upwelling regions, where productivity is high, evasion of gaseous elemental mercury is diminished due to scavenging and sedimentation of Hg by organic particles. In this study, we compared Hg concentrations and accumulation rates in the past ∼4,300 and 19,400 years derived from sediment cores collected in the Peruvian upwelling region (Peru Margin) and compared them with those of two other cores collected from the sediment fan of the Amazon and a core from the Congo Basin, which is influenced by both seasonal coastal upwelling and discharge from the river. Median Hg concentrations were higher at the Peru Margin (90.7 $\mu g\ kg^{-1}$) and in the Congo Basin (93.4 $\mu g\ kg^{-1}$) than in the Amazon Fan (35.8 $\mu g\ kg^{-1}$). The average Hg accumulation rates in sediments from the Peru Margin (178 $\mu g\ m^{-2}\ yr^{-1}$) were factors of ∼4 and ∼39 times higher than those from the Congo Basin (46.7 $\mu g\ m^{-2}\ yr^{-1}$) and Amazon Fan (4.52 $\mu g\ m^{-2}\ yr^{-1}$), respectively. Principal component analysis (PCA) of the geochemical data set reveals that Amazon Fan sediments are strongly influenced by the deposition of terrestrial material, which is of less importance in the Congo Basin and of minor importance in Peru Margin sediments. Accordingly, Hg export to sediments in upwelling areas largely surpasses that in fans of large rivers that drain large terrestrial catchments. The high Hg accumulation rates in the sediments from the upwelling area and the minor influence of terrestrial Hg fluxes there suggest that atmospheric-derived Hg in upwelling areas is effectively exported to the sediments through scavenging by organic particles.

Keywords: mercury accumulation, marine sediment core, river, upwelling, algal scavenging

OPEN ACCESS

Edited by:
Renato S. Carreira, Pontifical Catholic University of Rio de Janeiro, Brazil

Reviewed by:
Angela De Luca Rebello Wagener, Pontifical Catholic University of Rio de Janeiro, Brazil
Ruei-Feng Shiu, National Taiwan Ocean University, Taiwan

****Correspondence:***
Sara Zaferani
s.zaferani@tu-braunschweig.de

Specialty section:
This article was submitted to Marine Biogeochemistry, a section of the journal Frontiers in Marine Science

Received: *29 June 2021*
Accepted: *08 September 2021*
Published: *28 September 2021*

Citation:
Zaferani S and Biester H (2021) Mercury Accumulation in Marine Sediments – A Comparison of an Upwelling Area and Two Large River Mouths. Front. Mar. Sci. 8:732720. doi: 10.3389/fmars.2021.732720

INTRODUCTION

Hg is a toxic element that is globally dispersed from natural and anthropogenic sources. In the global biogeochemical Hg cycle, a substantial amount of Hg emitted to the atmosphere from natural and anthropogenic sources reaches the ocean (Horowitz et al., 2017; Schartup et al., 2019), and ocean sediments are regarded as the ultimate sink of Hg (Fitzgerald et al., 2007; Selin, 2009; Amos et al., 2013).

Hg input to the ocean primarily occurs through atmospheric deposition (Mason et al., 1994; Driscoll et al., 2013). After deposition, as either mercuric ions (Hg^{2+}) or elemental Hg (Hg^0), Hg can be (i) reduced to Hg^0 and evaded to the atmosphere, (ii) scavenged from the water column by particulate matter and eventually buried in deep-sea sediments, or (iii) methylated to either monomethylmercury (CH_3Hg^+) or dimethylmercury [$(CH_3)_2Hg$] (Mason et al., 2012; Lamborg C. et al., 2014). The resulting CH_3Hg^+ is a neurotoxin that bioaccumulates and biomagnifies in marine food webs (Lamborg C. et al., 2014). The main pathway of human exposure to methylmercury is primarily through the consumption of marine fish (Jensen and Jernelöv, 1969; Mahaffey et al., 2011; Mason et al., 2012; Schartup et al., 2018). Although coastal and shelf sediments were believed to be the main methylmercury source for marine fish (Fitzgerald et al., 2007), recently methylation has been also observed in well-oxygenated surface waters (Heimburger et al., 2015; Schartup et al., 2015).

Unlike the well-studied Hg cycling in terrestrial environments, our understanding of the fate of Hg in the oceans is still limited and especially lacks data from Hg accumulation in different marine sedimentary systems. Available information about the global Hg burial in ocean sediments is mainly based on model estimates (Mason and Sheu, 2002; Sunderland and Mason, 2007; Outridge et al., 2018) and water measurements (Cossa et al., 2011; Lamborg C. H. et al., 2014; Heimburger et al., 2015; Kim et al., 2017). It has been estimated that approximately 96% of the deposited Hg to the ocean is lost through evasion from the surface, and only 30% of the Hg flux that reaches the deep ocean is preserved in sediments (Mason and Sheu, 2002). However, a recent study of isotope mass balance suggests that evasion flux estimations from models are likely overestimated (Jiskra et al., 2020). The current estimate of deep-ocean Hg accumulation also shows that Hg flux in the deep ocean is higher than the currently accepted deep-ocean average Hg flux (Sanei et al., 2021).

There are contradictory statements about Hg deposition and evasion to/from different surface waters. One type of area in particular that highlights this uncertainty is upwelling regions. Upwelling regions are some of the most productive marine ecosystems worldwide (D'Croz and O'Dea, 2007) and consequently important areas for the global fishery (Chavez et al., 2008). This is due to the upwelling of deep water, which brings nutrients to the surface waters of the ocean. Most available data on Hg behavior in upwelling regions are based on model estimates (Kim and Fitzgerald, 1986; Soerensen et al., 2014; Mason et al., 2017). There are only a few sediment measurements that only go as far back as the previous century (Figueiredo et al., 2013). Some studies have suggested that Hg evasion is high in productive upwelling regions of the ocean due to enhanced biological reduction (Fitzgerald et al., 1984; Mason and Fitzgerald, 1993). Other studies have suggested lower Hg evasion in productive regions (O'Driscoll et al., 2006; Qureshi et al., 2010; Soerensen et al., 2013, 2014). These studies have found relatively low concentrations of atmospheric and surface water-phase Hg^0 in regions with high productivity compared with areas with low productivity. These studies have related their observations to the sorption and scavenging of Hg by suspended organic particles. They have suggested that the removal of Hg^{2+} associated with sorption and scavenging by suspended organic particles in productive regions decreases the amount of available Hg^{2+} for reduction and re-emission. Figueiredo et al. (2013) attributed the relatively high Hg flux in their study area to high productivity and organic matter deposition.

The mechanism of Hg uptake or scavenging by phytoplankton or related debris is not well-understood. Nevertheless, it has been demonstrated that Hg–phytoplankton interactions can affect Hg cycling by influencing its speciation, concentrations, and flux from the water column to sediments (Mason et al., 1996; Le Faucheur et al., 2014). This is confirmed by water column measurements that showed a nutrient-like distribution of Hg in the water column of oceans (Cossa et al., 2011, 2018; Lamborg C. H. et al., 2014; Bowman et al., 2015; Munson et al., 2015). These studies observed that Hg in the ocean behaves the same way as nutrients. Similar to macronutrients, Hg shows higher concentrations in deep water owing to its release during organic matter decomposition (Lamborg C. H. et al., 2014). The role of biological productivity on Hg accumulation in ocean sediments is not well constrained yet. This is due to a scarcity of marine sediment data (Zaferani et al., 2018). Thus far, it has been shown that the scavenging of Hg by algae is the major vector for Hg burial in the sediment of marine Antarctica with high levels of primary productivity (Zaferani et al., 2018). However, its role in the accumulation of Hg in sediments in upwelling areas is poorly understood.

In addition to atmospheric deposition, Hg enters the ocean *via* rivers. Some studies have indicated that, on a global scale, Hg export to the oceans by rivers is small (Lamborg et al., 2002; Strode et al., 2007). Other studies have indicated that Hg inputs to marine ecosystems by rivers are large (Sunderland and Mason, 2007; Amos et al., 2014; Zhang et al., 2015). According to these studies, the amount of Hg discharged by rivers to ocean margins is comparable to the input from atmospheric deposition to the global ocean (Amos et al., 2014; Zhang et al., 2015). Some studies have considered benthic sediment at ocean margins as a sink for most river-derived Hg, owing to the bounding of Hg to particles (Chester, 2003). Other investigations have indicated that the amount of Hg burial in ocean margins differs among regions and depends on freshwater discharge rates and the physical characteristics of different estuaries (McKee et al., 2004). Similar to that about upwelling regions, knowledge about the impacts of rivers on the marine Hg cycle is limited to model calculations. These contradictory assumptions reflect uncertainty in model parameters due to data limitations.

The objective of this study was to compare Hg accumulation in marine regions influenced by upwelling and related high primary

productivity and Hg input by large rivers with large terrestrial catchments. To do so, we investigated sediment cores from the Peru Margin (a core located in the upwelling zone), Congo Basin (a core located in an environment dominated by freshwater input from the Congo River and seasonal coastal upwelling), and Amazon Fan (a core from the mouth of the Amazon River). To decipher sources and driving factors controlling the sequestration of Hg in these sediments, we combined data on Hg accumulation with those derived from multielement analyses and PCA.

MATERIALS AND METHODS

Study Sites and Core Collections

Congo Basin

In 1997, sediment core 1076A was collected from the Lower Congo Basin (5° 4.132′S, 11° 6.092′E, 204.3-m-long sediment core, 1,404.2 m water depth) during Ocean Drilling Program (ODP) Expedition 175 using an advanced hydraulic piston corer (**Figure 1**). The core falls within the Angola–Benguela Current system, which is one of the great upwelling regions in the world (Wefer et al., 1998). This region is also influenced by freshwater input from the Congo River. The sediment along the core comprises bioturbated organic carbon-rich olive-gray clay and greenish-gray clay. Biogenic sections contain abundant diatoms with rare nanofossils, silicoflagellates, siliceous sponge spicules, phytoliths, and traces of radiolarian and foraminifer fragments. The core was sliced by 5 cm^3 plastic scoops into 1 cm slices. Samples from the upper 1 m of the core were collected at ∼1 cm intervals, resulting in a total of 99 samples, representing the past ∼5,000 years (Wefer et al., 1998).

Peru Margin

Sediment core 1228B was collected from the continental shelf of Peru (11° 3.862′S, 78° 4.664′W, 55.3-m-long sediment core, 262.3 m water depth) in 2002 during ODP Expedition 201 using a hydraulic piston corer (**Figure 1**). Site 1228 lies within the Peru upwelling zone. Winds along the coast of Peru maintain the upwelling process throughout the year. Strong upwelling of cold, nutrient-rich subsurface water causes extensive phytoplankton blooms and high productivity in this region, which is known as the Peruvian high-productivity upwelling system (Tarazona and Arntz, 2001; D'Hondt et al., 2003). The continental shelf of Peru has been dominated by upwelling over the last 40 kyr. Sediments are predominantly biogenic sediments and silt and clay-sized, predominantly siliciclastic sediments. Large, fast-growing diatoms dominate the phytoplankton biomass (De Mendiola, 1981; Scheidegger and Krissek, 1983; DiTullio et al., 2005). Samples from the upper 2.70 m of the core were collected at ∼10 cm intervals, resulting in a total of 27 samples, representing the past ∼4,300 years (D'Hondt et al., 2003).

Amazon Fan

Sediment core 941A was collected from the western side of the Amazon Fan, at the mouth of the Amazon River (5°22.384′N, 48°1.723′W, 177.66-m-long sediment core, 3,380.9 m water depth), in 1994 during ODP Expedition 155. The fan contains much material eroded from the continent within the Amazon drainage basin and fluvial sediments (Flood et al., 1995). The sediments consist of bioturbated nanofossil-foraminifera clay and carbonate. Samples from the upper 1 m of the core were collected at ∼1 cm intervals, resulting in a total of 93 samples, representing the past ∼19,400 years (Flood et al., 1995).

Analysis

All solid samples were freeze-dried and hand-ground using a mortar and pestle before geochemical analysis.

Carbon, Nitrogen, and Sulfur

Total carbon (C), nitrogen (N), and sulfur (S) were analyzed using a EuroEA 3000 elemental analyzer (Hekatech GmbH, Germany). Carbonate in the samples was removed with HCl acid. The quality of the analysis was ensured by certified reference materials (CRMs), i.e., sulphanilamide (C = 41.75 ± 0.17%; N = 16.26 ± 0.22%; S = 18.64 ± 0.18%), BBOT 2.5-Bis(5-tert-butyl-benzoxazol-2-yl)thiophene (C = 72.52%; N = 6.51%; S = 7.44%), Canmet LKSD-4 lake sediment (C = 17.7 ± 0.8%; S = 0.99 ± 0.09%), and MOC soil standard (C = 3.19 ± 0.07%). The average results for the CRMs were sulphanilamide (n = 31) C = 42.0 ± 0.25%, N = 16.2 ± 1.01%, and S = 18.5 ± 0.54%; BBOT (n = 6) C = 72.2 ± 0.12%, N = 6.55 ± 0.04%, and S = 7.41 ± 0.03%; LKSD-4 (n = 5) C = 19.1 ± 0.05% and S = 1 ± 0.01%; and MOC (n = 6) C = 3.23 ± 0.02%.

Mercury Analysis

Total Hg was determined by thermal decomposition followed by preconcentration of Hg on a gold trap and cold vapor atomic absorption spectrometry (CVAAS) Hg detection using a Milestone DMA-80 analyzer (EPA, 1998). The quality of the analysis was ensured by including a CRM (Canmet LKSD-4 = 190 ± 17 ng g^{-1}) alongside the analyzed samples. The average measured concentration for LKSD-4 (n = 37) was 190 ± 15 ng g^{-1}. The results of replicate analyses (n = 27) were always within a relative standard deviation (RSD) of 10% of the certified value.

Major and Trace Element Analysis

The samples were analyzed for concentrations of silicon (Si), titanium (Ti), zirconium (Zr), sulfur (S), calcium (Ca), potassium (K), aluminum (Al), yttrium (Y), manganese (Mn), strontium (Sr), iron (Fe), lead (Pb), copper (Cu), zinc (Zn), arsenic (As), bromine (Br), nickel (Ni), chlorine (Cl), and rubidium (Rb) by energy dispersive X-ray fluorescence (ED-XRF). The methods used for calibration and accuracy and precision determination are described in detail in Cheburkin and Shotyk (1996). The CRMs (Canmet LKSD-4, NRC/CNRC-PACS-2, NRC/CNR-Mess-3, and NCS-DC75304) and replicates were measured in each set of samples for accuracy and precision control. Repeated analysis of CRMs gave an RSD of less than 10% for Si, K, Ca, Ti, Mn, Fe, Zn, Br, Rb, Sr, Y, and Zr; 8 –17% for Ni, Cu, Cl, and S; 6–15% for Al and Ba; 4–12% for Pb; and 9–20% for As.

Statistical Analyses

PCA was applied to the major and trace element concentrations to identify processes controlling the variability of elements

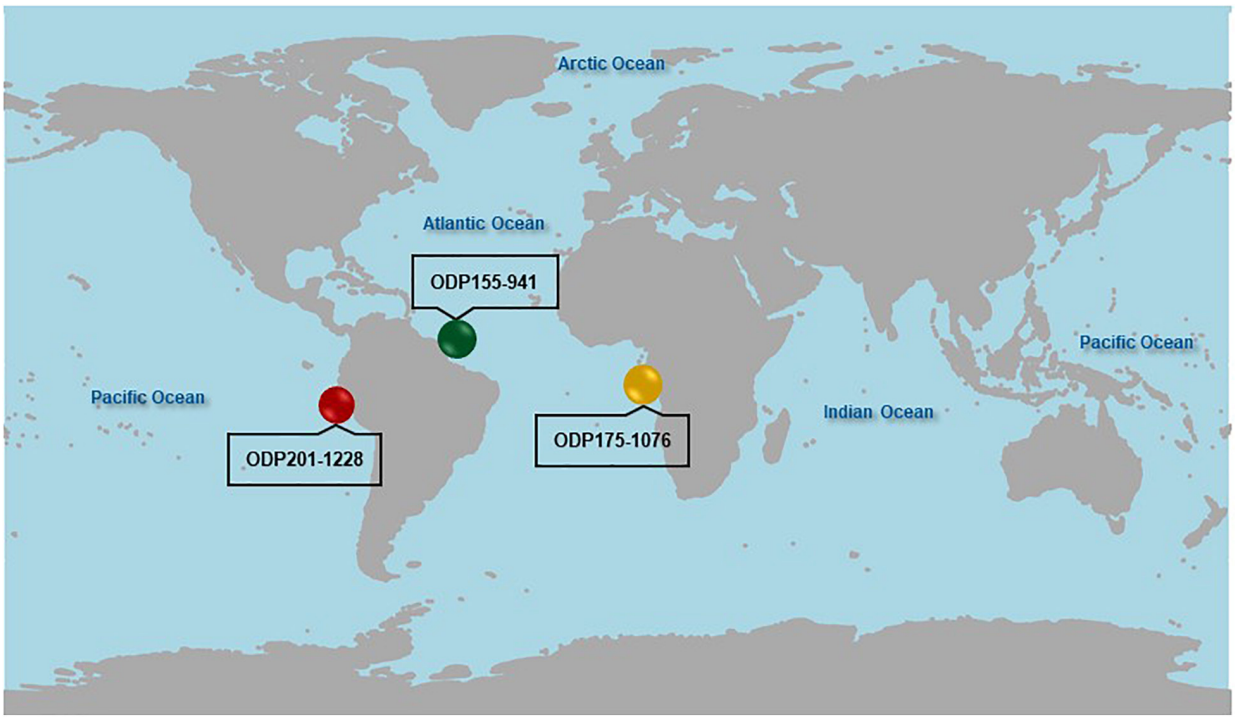

FIGURE 1 | Locations of the ODP175-1076 core in the Congo Basin, ODP201-1228 core in the Peru Margin, and ODP155-941 core in the Amazon Fan.

in the sediments. When there is a complex set of variables, PCA is used to reduce a large number of variables to a new set of artificial variables, called principal components. Each component includes variables with a similar downcore pattern. The principal components are then interpreted in terms of relevant geochemical processes that can control the variability of the major and trace elements in the sediments. The derived interpretation from PCA was then combined with the Hg data to examine the processes that could affect Hg accumulation. The analysis was performed on the standardized concentration data using Z scores (expressed in terms of standard deviations from their means). Correlation analysis and PCA were performed using the statistical software SPSS 25.0.

RESULTS AND DISCUSSION

Geochemical Processes Controlling the Distribution of Elements in the Sediments

Congo Basin

The correlation matrix of elements and concentration profiles of Si, Zr, Al, K, Ti, Br, S, Sr, Ca, C, and Zn and C/N ratios are shown in **Supplementary Table 1** and **Figure 2**, respectively. Si has the highest concentration of all elements in the sediments of the Congo Basin. On the one hand, Si is associated with the flux of terrestrially derived mineral components and, on the other hand, with siliceous phytoplankton, protozoans, protists, plant phytoliths, and sponge spicules (Croudace and Rothwell, 2015). The record of Si concentrations does not show a specific trend and varies between 13.3 and 20.7%, with a median of 15.9%. The records of Al, Ti, Cl, K, S, Mn, and Ca follow the Si concentration trend. Concentrations of Al, Ti, Cl, K, S, and Ca range between ∼3.24 and 8.89%, ∼3,136 and 6,432 mg kg^{-1}, 1.24 and 2.89%, ∼0.78 and 1.59%, ∼0.34 and 0.80%, and ∼0.59 and 0.91%, respectively. The positive covariance of Al and Ti, as lithogenic elements, with the abovementioned elements reveals that fluctuations in these elemental concentrations in Congo Basin sediments are likely related to changes in terrestrial inputs. This can be due to fluctuations in Congo River discharge. The records of Ni, Fe, Cu, Zn, Br, and Sr concentrations show similar trends throughout the core (**Figure 2**). Ni, Fe, Cu, Zn, Br, and Sr concentrations vary between ∼31.8 and 75.8 mg kg^{-1}, ∼6.65 and 13.1%, ∼19.7 and 48.3 mg kg^{-1}, ∼92 and 169 mg kg^{-1}, ∼167 and 248 mg kg^{-1}, and ∼87.3 and 105 mg kg^{-1}, respectively. The covariation of Fe, Ni, Cu, and Zn, as biologically essential elements (Morel and Price, 2003), suggests that fluctuations of these elements are mainly associated with the biological production and settling of biogenic debris. In the Congo Basin, biological productivity is mainly the result of upwelling (Wefer et al., 1998). The organic C concentration varies between ∼2.76 and 4.01%, with a median of 3.23%. This concentration is higher than that in most deep-sea sediments from the South Atlantic (∼0.3 wt%) (Premuzic et al., 1982; Keswani et al., 1984) and reflects a history of elevated primary production in this area caused by upwelling (Wefer et al., 1998). C/N ratios vary by a factor of ∼1.27 between 11.5 and 14.6 at

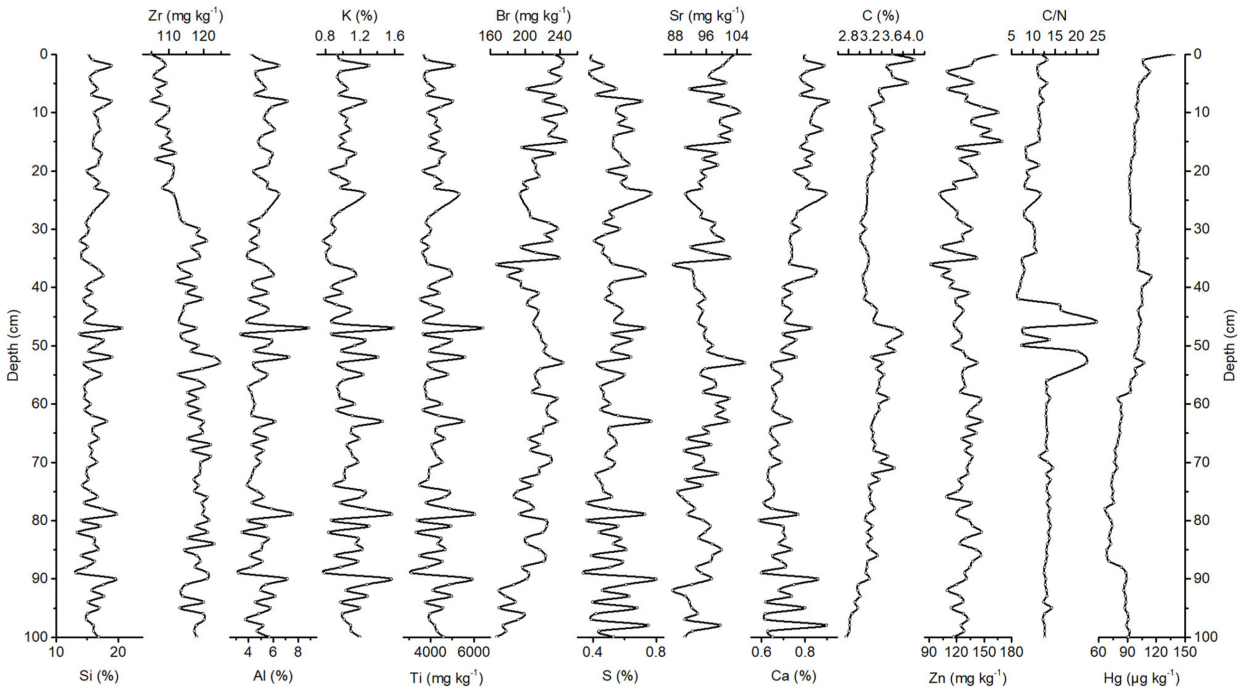

FIGURE 2 | Downcore records of Si, Zr, Al, K, Ti, Br, S, Sr, Ca, C, Zn, and Hg concentrations and C/N ratios of Congo Basin sediments.

a 100–56 cm depth and by a factor of ∼2.13 between 6.46 and 13.8 at a 50–1 cm depth of the core, with five more pronounced peaks at approximately 53, 51, 46, 44, and 43 cm depths. A shift in the C/N ratio from relatively higher values (median: 13.2) in the lower ∼50 cm of depth to lower values (median: 10.4) in the upper ∼50 cm depth of the core indicates a change in the source of organic matter from terrestrial sources (higher C/N ratios) to marine sources (lower C/N ratios). This change is likely attributable to the change in environmental conditions and increasing input from the Congo River in the lower 50 cm depth of the core. Stronger freshwater discharge from the Congo River is a result of a more intense monsoon over Central Africa and enhanced precipitation (Uliana et al., 2002).

The PCA for the Congo Basin data set resulted in five components (**Table 1** and **Supplementary Figure 1**), explaining almost 82% of the total variance. The first component (Cp1) explains 33% of the variance and shows large positive loadings for Si, Ti, Al, K, Cl, S, and Mn. The second component (Cp2), which explains 21% of the variance, is characterized by large positive loadings for Fe, Cu, Ni, Sr, Zn, and Br. The third component (Cp3) explains 16% of the variance and shows large positive loadings for Hg, N, Ca, and Mn and negative loadings for Rb and Zr. The fourth and fifth components (Cp4 and Cp5) account for 6 and 5% of the variance, respectively. Cp4 is characterized by positive loadings for C, and Cp5 shows positive loadings for Pb. In general, the PCA results imply that Congo Basin sediments are formed by material from terrigenous (Congo River) and biogenic (Benguela upwelling) sources.

Briefly, Cp1, which mainly includes positive loadings of lithogenic elements, represents the variability of terrigenous and fluvial inputs from the Congo River. Cp2 mainly comprises loadings of elements of biogenic sources and appears to reflect biogenic productivity. Cp3 appears to reflect biogenic productivity, mainly calcite-producing microorganisms, as a result of upwelling. Increased biogenic fluxes are accompanied by relative dilution of the terrigenous content of the sediments. This is reflected by the negative loadings for Rb and Zr, as indicators of changes in the flux of lithogenic materials, in Cp3. Hg forms a group along Cp3 together with positive loadings for biogenic sources and negative loadings for terrigenous sources. Cp4, which includes positive loading for C, represents the variability of primary productivity as well.

Peru Margin

The correlation matrix of elements and concentration profiles of Si, Zr, Al, K, Ti, Br, S, Sr, Ca, C, and Zn and C/N ratios are shown in **Supplementary Table 2** and **Figure 3**, respectively. Similar to that in the Congo Basin, Si has the highest concentration of all elements in the sediments of the Peru Margin. Si can be detrital, derived from the weathering of crustal rocks, or biogenic, derived from siliceous phytoplankton (Croudace and Rothwell, 2015). The record of Si concentrations shows an increasing trend from the top to the bottom of the core and varies between 14.6 and 27.4%, with a median of 18.3%. The records of K, Zr, Ti, Al, and Y concentrations generally follow the Si concentration trend. Concentrations of K, Zr, Ti, Al, and Y range between ∼0.52 and 1.47%, ∼41.7 and 219 mg kg^{-1}, ∼1,219 and 3,057 mg kg^{-1}, ∼2.27 and 4.41%, and ∼11.6 and 24.5 mg kg^{-1}, respectively. Zr, as a conservative lithogenic element, is an indicator of changes in the flux of terrestrial material. The positive correlations of

Zr with the abovementioned elements, therefore, indicate that they are associated with terrestrial inputs as well. Organic C was found to be another major component in these sediments and is associated with the Peruvian high-productivity upwelling system. Concentrations vary between ∼2.58 and 15.9%, with a median of 13.1%. The organic C concentrations record shows a decreasing trend from the top to the bottom of the core. Sea level fluctuations and the associated shift of bottom circulation and the oxygen minimum layer can be the main reasons for the decreasing trend in organic C (Suess and von Huene, 1988). The C/N ratios in the Peru Margin sediments vary between 8.89 and 10.5, with 2 more pronounced peaks at depths of approximately 200 and 190 cm in the core. Low C/N ratios indicate that marine organic matter is the source of organic matter in the Peru Margin sediments. This is a result of high primary productivity in the surface water driven by upwelling. The variability in the C/N ratio record is generally low in Peru Margin sediment (**Figure 3**), pointing to non-significant changes in terms of the dominant source of organic matter. The records of Ni, Br, Cu, Zn, and Cl concentrations show a similar trend to the organic C concentration. Ni, Cu, and Zn are known to have a biological role (Morel and Price, 2003). Concentrations of Ni, Cu, and Zn range between ∼12.8 and 180 mg kg^{-1}, ∼11 and 95 mg kg^{-1}, and ∼65.6 and 182 mg kg^{-1}, respectively. Br is also associated with marine organic matter and related productivity (Ziegler et al., 2008, 2009; Ren et al., 2009; Caley et al., 2011). The concentration of Br ranges between ∼45 and 1,577 mg kg^{-1}. Cl can travel through biological pathways (incorporation into algae) and reach the sediments by fast-sinking detritus (Leri et al., 2015). Concentrations vary between ∼1.14 and 5.21%. Correlations of the abovementioned elements with organic C reflect the same depositional process, which is accumulation by organic matter flux from surface waters.

The PCA results further helped explain the processes that affected Peru Margin sedimentation. The PCA yielded five components (**Table 2** and **Supplementary Figure 2**), explaining almost 92% of the total variance. Cp1 explains 52% of the variance and shows large positive loadings for Cl, S, Cu, Ni, N, and C and negative loadings for Y and Zr. Cp2, which explains 18% of the variance, is characterized by large positive loadings for Hg, Rb, Br, N, Zn, and C and negative loading for Si. Cp3 explains 12% of the variance and shows large positive loadings for Si, Ti, K, Mn, and Al. Cp4 and Cp5 account for 7 and 4% of the variance, respectively. Cp4 is characterized by positive loadings for Ca and Sr and negative loading for Pb. Cp5 shows positive loadings for Fe and As.

The PCA results imply that mainly terrigenous material input, upwelling productivity, and associated particle export to the seafloor affected Peru Margin sedimentation. Briefly, Cp1 and Cp2, which include positive loadings for elements associated with biogenic productivity, appear to reflect the productivity in the upwelling system and associated particle export to the seafloor. The covariation of Ni and Cu with organic C along Cp2 implies that for this component, the main removal mechanism is settling with organic matter (Böning et al., 2015). Increased biogenic fluxes are accompanied by dilution of the terrestrial matter content, which is reflected by the negative loadings for Y and Zr along Cp1 and Si along Cp2. The variance of Hg was captured by this component. Cp3, which includes positive loadings for lithogenic elements, represents the variability of terrigenous inputs. The Peru Margin site, unlike our two other sites, i.e., the Congo Basin and Amazon Fan, is not affected by riverine discharge (D'Hondt et al., 2003). Sources of terrigenous sediments to the Peru Margin are controlled primarily by continental supplies (Jaisi and Blake, 2010). The covariation of Ca and Sr in Cp4 represents marine productivity, mainly that of foraminifers and coccolithophorids. Cp1 and Cp2 account for much of the variability/process that controlled the geochemical composition of these sediments. This information, along with knowing that the Peru Margin site is a major upwelling site and receives a very small amount of riverine discharge, suggests that the contribution of terrigenous inputs is small.

TABLE 1 | Factor loadings for the five significant components extracted by PCA from Congo Basin sediment samples.

Variables	Components				
	1	2	3	4	5
Si	**0.96**	−0.14	0.09	0.09	0.02
Ti	**0.96**	−0.13	−0.06	−0.08	−0.03
Al	**0.93**	−0.13	0.15	0.02	0.02
K	**0.91**	−0.14	−0.33	0.06	−0.03
Cl	**0.87**	−0.02	0.17	0.32	0.17
S	**0.81**	−0.08	0.20	−0.23	−0.03
Fe	−0.17	**0.90**	−0.09	−0.16	0.11
Cu	−0.13	**0.83**	−0.12	−0.02	−0.05
Ni	−0.15	**0.81**	−0.11	−0.10	−0.13
Sr	0.00	**0.79**	0.22	0.37	−0.02
Zn	−0.04	**0.79**	−0.16	0.28	0.20
Br	−0.07	**0.77**	0.14	0.52	0.12
Rb	−0.03	0.25	**−0.91**	−0.01	−0.11
Hg	−0.05	0.02	**0.85**	0.17	0.00
N	−0.01	−0.02	**0.71**	−0.06	−0.03
Ca	0.57	0.10	**0.69**	0.14	0.15
Mn	**0.64**	−0.03	**0.67**	0.03	0.09
Zr	−0.18	0.08	**−0.64**	−0.47	−0.30
C	0.04	0.16	0.11	**0.86**	−0.05
Pb	0.02	0.44	0.04	−0.17	**0.75**
Y	−0.07	0.40	−0.25	−0.23	−0.59
Eigenvalue	6.94	4.47	3.41	1.33	0.99
%Variance	33	21	16	6	5

Significant values are in bold.

Amazon Fan

The correlation matrix of elements and concentration profiles of Si, Zr, Al, K, Ti, Br, S, Sr, Ca, C, and Zn and C/N ratios are shown in **Supplementary Table 3** and **Figure 4**, respectively. Si has the highest concentration of all elements in the sediments from the Amazon Fan. The record of Si concentrations shows no specific trend with depth and varies between 17.3 and 23%, with a median of 20.5%. The records of Ti, Y, Rb, Zn, and Fe concentrations generally show a similar tendency and increase from the top to the bottom of the core. Concentrations of Ti, Y, Rb, Zn, and Fe range between ∼2,871 and 5,129 mg kg^{-1}, ∼16.7

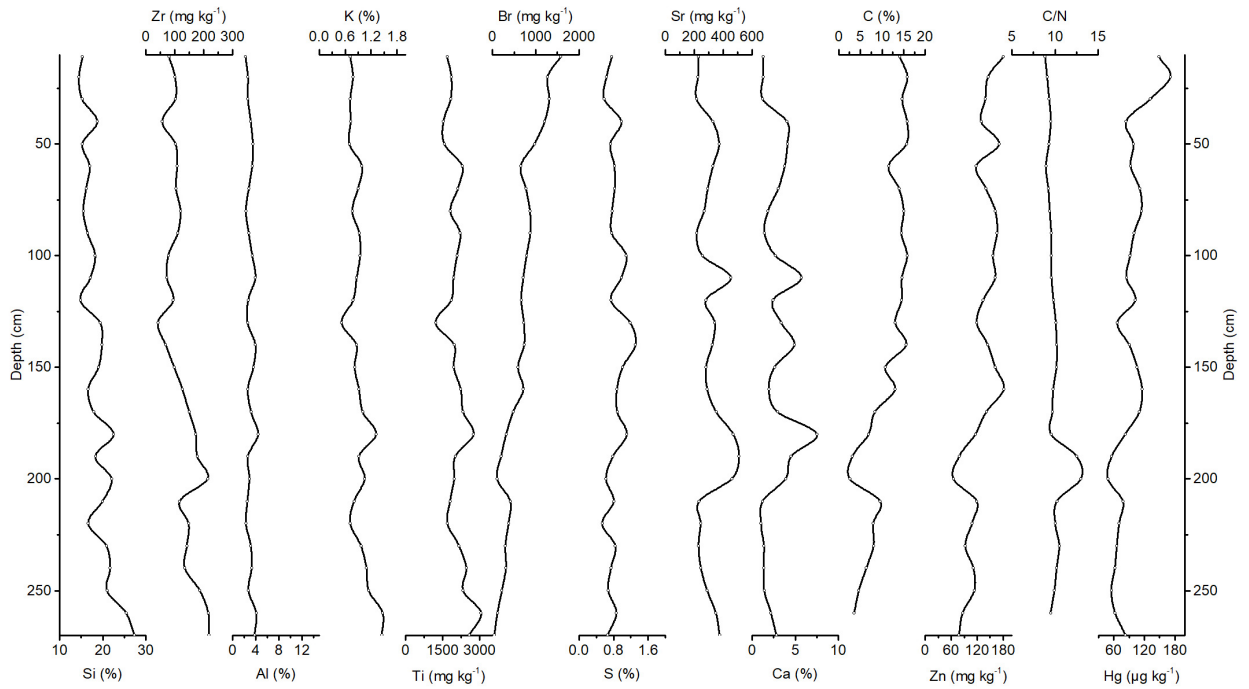

FIGURE 3 | Downcore records of Si, Zr, Al, K, Ti, Br, S, Sr, Ca, C, Zn, and Hg concentrations and C/N ratios of Peru Margin sediments.

and 26.2 mg kg^{-1}, ∼75.2 and 143 mg kg^{-1}, ∼62.8 and 146 mg kg^{-1}, and ∼2.21 and 8.24%, respectively. Covariations of Ti, as a proxy for the changes in the flux of lithogenic material, with the mentioned elements indicate an association of these elements with terrigenous inputs from the catchment of the Amazon River. Sr concentrations fluctuate by a factor of approximately two between ∼200 and 317 mg kg^{-1} within a 97–70 cm depth range of the core. At a depth of 70 cm, the concentration increases by a factor of approximately 4 and reaches 223 to 1,033 mg kg^{-1}. Sr concentrations fluctuate by a factor of approximately 1.7 between 622 and 1,041 mg kg^{-1} from a 42 cm depth to the top of the core. The record of Ca shows a similar pattern to the record of Sr. Ca concentrations fluctuate by a factor of approximately 2 between ∼1.96 and 4.09% within a 97–70 cm depth range. At a depth of 70 cm, the Ca concentration increases by a factor of approximately 7 and reaches 2.67–18.7%. Ca concentrations fluctuate by a factor of approximately 1.8 between 10.1 and 18.6% from 42 cm to the top of the core. Hence, Sr is a proxy for biogenic origin, covariation of Ca with Sr reflecting the fact that Ca is mainly biogenic and that they are associated with calcite-producing microorganisms. Variations in Ca and Sr reflect dilution by terrigenous material rather than productivity changes. This is indicated by the negative correlations of these two elements with lithogenic elements. Varying fluxes of terrestrial material resulted in the dilution of calcite organisms in the sediments. After Si, Ca has the highest average concentration and is found to be another major component in the sediments from the Amazon Fan. This can be associated with foraminifers (Flood et al., 1995) and indicates that calcite-producing microorganisms contribute significantly to the Amazon Fan sediments. Organic C concentrations vary between ∼0.51 and 0.94%, with a median of 0.64%. The average organic C concentrations in the Amazon Fan are a factor of 5 and 17 times lower than those in the Congo Basin and Peru Margin, respectively. The variability in C/N ratios is generally low. The ratios vary by a factor of ∼1.66 between 8.33 and 13.8, with a median of 10.1. Concentrations of biologically essential elements such as Zn, Ni, Cu, and Fe vary between ∼62.8 and 146 mg kg^{-1}, ∼14.4 and 46.8 mg kg^{-1}, ∼15.6 and 54.1 mg kg^{-1}, and ∼2.21 and 8.24%, respectively.

The PCA yielded five components (**Table 3** and **Supplementary Figure 3**), explaining almost 83% of the total variance. Cp1 explains 44 % of the variance and shows large positive loadings for Rb, Y, Pb, Zn, Ti, Fe, Hg, and Ni and negative loadings for Ca, Sr, and Al. Cp2, which explains 14% of the variance, is characterized by large positive loadings for K, Si, Cl, and S. Cp3 explains 11% of the variance and shows large positive loadings for Ni, Mn, and Cu. Cp4 and Cp5 account for 8 and 6 % of the variance, respectively. Cp4 is characterized by positive loadings for C, N, and Br. Cp5 shows positive loadings for As and Zr.

Record of Mercury Accumulation

Congo Basin

Based on the age models and estimated sedimentation rate of 20 cm kyr^{-1} for the Congo Basin (Wefer et al., 1998), sediments in the top 98 cm of the core correspond to approximately 5,000 years.

In this period, Hg concentrations range between 67.2 and 139 µg kg^{-1}, with a median of 93.4 µg kg^{-1}. Hg concentrations fluctuate between 84 and 92.5 µg kg^{-1} within a 98–88 cm depth range of the core (**Figure 2**). At 87 cm, the Hg concentration decreases by a factor of approximately 1.2 and

TABLE 2 | Factor loadings for the five significant components extracted by PCA from Peru Margin sediment samples.

Variables	Components				
	1	2	3	4	5
Cl	**0.91**	0.15	−0.21	0.18	0.01
Y	**−0.84**	−0.12	0.40	0.13	−0.06
Zr	**−0.80**	−0.35	0.42	−0.01	−0.10
S	**0.79**	−0.21	0.27	0.39	0.10
Cu	**0.75**	0.32	−0.31	−0.04	0.42
Ni	**0.64**	0.53	−0.27	−0.05	0.40
Hg	0.14	**0.87**	−0.11	−0.15	0.11
Rb	−0.23	**0.81**	0.09	−0.32	0.33
Br	0.45	**0.75**	−0.38	−0.10	−0.01
N	**0.60**	**0.69**	−0.33	−0.02	0.12
Si	−0.12	**−0.66**	**0.64**	0.00	−0.24
Zn	0.47	**0.64**	−0.15	−0.03	0.50
C	**0.64**	**0.64**	−0.34	−0.01	0.13
Ti	−0.39	−0.06	**0.89**	0.00	0.05
K	−0.43	−0.23	**0.85**	0.07	−0.07
Mn	−0.49	−0.22	**0.82**	−0.01	−0.04
Al	0.21	−0.12	**0.78**	0.46	−0.09
Ca	0.20	−0.11	0.20	**0.93**	−0.09
Sr	−0.21	−0.34	0.12	**0.87**	−0.11
Pb	−0.15	−0.21	0.46	**−0.61**	0.38
Fe	0.11	0.32	0.08	−0.29	**0.87**
As	0.56	0.22	−0.25	−0.08	**0.64**
Eigenvalue	11.5	3.87	2.58	1.57	0.79
%Variance	52	18	12	7	4

Significant values are in bold.

reaches 71 $\mu g\ kg^{-1}$. At this depth of the core, the Hg record shows an increasing trend to the top of the core and reaches 114 $\mu g\ kg^{-1}$ at a core depth of 38 cm. At a core depth of 37 cm, the Hg concentration decreases by a factor of approximately 1.1 and reaches 101 $\mu g\ kg^{-1}$. Hg concentrations fluctuate between 92.2 and 113 $\mu g\ kg^{-1}$ within a 37–1 cm depth range of the core and reach a maximum value of 139 $\mu g\ kg^{-1}$ at the very top of the core. The estimated average Hg accumulation rate in the Congo Basin is ∼46.7 $\mu g\ m^{-2}\ yr^{-1}$.

To identify driving forces of the variations in Hg accumulation, we used the regression analysis of the C/N ratios and Hg concentrations (**Supplementary Figure 4**), our PCA results (**Table 1**), and the correlation matrix of elements (**Supplementary Table 1**). The variance in Hg in the Congo Basin is captured by Cp3. We interpreted Cp3 as representing the variability of biogenic fluxes from upwelling productivity. This is indicated by positive loadings for N and Ca and negative loadings for Rb and Zr. PCA demonstrated that upwelling and enhanced marine productivity, mainly of foraminifers and coccolithophorids (Croudace and Rothwell, 2015), controlled the flux of Hg to Congo Basin sediments. PCA further revealed that Hg shows no positive covariance with lithogenic elements (e.g., Al, Ti, and K along Cp1). This indicates that terrestrial influence, associated with the supply by the Congo River, on Hg accumulation in these sediments is of minor importance.

Comparison of the Hg concentration record with the C/N ratio record indicates that in the lower 50 cm of the core, where C/N ratios are higher (median: 13.2), Hg concentrations are lower (median: 80.9 $\mu g\ kg^{-1}$), and in the upper 50 cm of the core, where C/N ratios are lower (median: 10.3), Hg concentrations are higher (median: 101 $\mu g\ kg^{-1}$). As mentioned above, the lower C/N ratios indicate a marine source for the organic matter.

No positive covariance of Hg with lithogenic elements, together with the information regarding the organic matter source, which was revealed from C/N ratios, and their relations with Hg concentrations, indicate that atmospheric Hg deposition and binding of atmospheric-derived Hg to marine-derived organic matter is the main source of Hg in Congo Basin sediments. The upwelling-related productivity in the Congo Basin increases Hg scavenging by organic particles and Hg export to the sediment.

Peru Margin

Considering a sedimentation rate of 85 cm kyr^{-1} for the Peru Margin, i.e., based on radiocarbon dating (D'Hondt et al., 2003), sediments in the top 270 cm of the core likely correspond to the past 4,300 years.

The Hg record at this time shows an increasing trend from the bottom to the top of the core. Hg concentrations range between 49 and 172 $\mu g\ kg^{-1}$, with a median of 90.7 $\mu g\ kg^{-1}$. The Hg concentration reaches a maximum value of 172 $\mu g\ kg^{-1}$ at a depth of 20 cm (**Figure 3**). The average Hg accumulation rate in Peru Margin is ∼178 $\mu g\ m^{-2}\ yr^{-1}$.

The results of the regression analysis of the C/N ratios and Hg concentrations (**Supplementary Figure 5**), the PCA (**Table 2**), and the correlation matrix of elements (**Supplementary Table 2**) helped identify the processes that controlled Hg sedimentation in the Peru Margin. Hg forms a group with high factor loadings along Cp2 together with Ni, Rb, Br, N, Zn, and C. The covariation of Hg with Ni, Cu, and organic C implies that the main removal mechanism of Hg in the Peru Margin is the sinking of plankton particles derived from productive surface waters of the Peru Margin. Hg shows no positive covariance with lithogenic elements (e.g., Al, Ti, and Zr). This indicates that terrestrial influences on Hg accumulation are negligible.

The C/N ratio record and its comparison with the Hg concentration record suggest that, similar to the pattern observed for Congo Basin sediment, the source of organic matter can influence Hg sedimentation. Low C/N ratios in the Peru Margin sediments, which point to a marine source for the organic matter, result from the settling of algae as a result of upwelling. Periods of low Hg concentrations, at approximately 200 and 190 cm in the core (**Figure 3**), correspond to phases of relatively high C/N ratios and relatively low marine organic matter. Similar to our conclusion for the Congo Basin, we conclude that the binding of atmospheric-derived Hg to sinking particles is the dominant process of Hg accumulation in these sediments.

Amazon Fan

Based on a sedimentation rate of 5 cm kyr^{-1} for the Amazon Fan (Flood et al., 1995), sediments in the top 97 cm of the core likely correspond to the past 19,400 years.

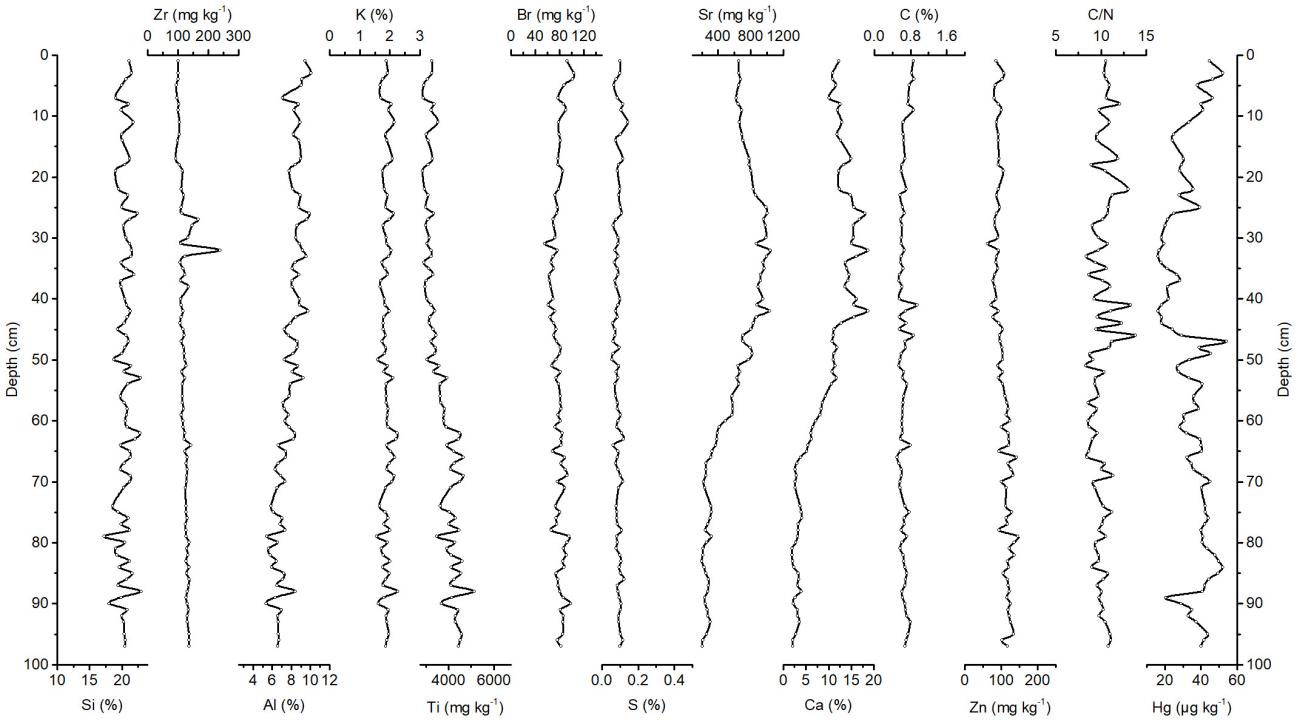

FIGURE 4 | Downcore records of Si, Zr, Al, K, Ti, Br, S, Sr, Ca, C, Zn, and Hg concentrations and C/N ratios of Amazon Fan sediments.

During this period, the Hg record shows no clear pattern with depth and ranges between 16.4 and 54 $\mu g\ kg^{-1}$, with a median of 35.8 $\mu g\ kg^{-1}$ (**Figure 4**). The Hg concentration decreases from 40 to 20.7 $\mu g\ kg^{-1}$ within a 97–89 cm depth range of the core. The Hg concentration increases at an 89 cm depth in the core and fluctuates between 27.3 and 54 $\mu g\ kg^{-1}$ within an 88–47 cm depth range of the core. At a depth of 47 cm, the Hg concentration decreases by a factor of ∼2.9 and reaches 18.4 $\mu g\ kg^{-1}$. The Hg record then shows a general increasing trend to the top of the core and ranges between 16.4 and 52 $\mu g\ kg^{-1}$. The average Hg accumulation rate in the Amazon Fan is ∼4.52 $\mu g\ m^{-2}\ yr^{-1}$.

To identify driving forces of the variations in Hg accumulation, we used the regression analysis of the C/N ratios and Hg concentrations (**Supplementary Figure 6**), our PCA results (**Table 3**), and the correlation matrix of elements (**Supplementary Table 3**). PCA results indicate that the variance of Hg in the Amazon Fan was captured by Cp1. Rb, Y, Pb, Zn, Ti, Fe, and Ni show positive factor loadings as well, whereas Ca, Sr, and Al show negative factor loadings. The covariation of Hg with terrigenous elements implies that Hg fluxes in the Amazon Fan are significantly influenced by changes in lithogenic inputs. Hg and Ca [Ca is attributed to biogenic carbonate in the Amazon Fan sediments (see section "Geochemical Processes Controlling the Distribution of Elements in the Sediments, Amazon Fan")] are negatively correlated (**Supplementary Table 3**). We hypothesize that this is due to the dilution effect rather than the negative covariation of Hg with groups of marine plankton such as foraminifera and coccolithophorids. The records of Hg concentrations in Amazon Fan sediments are not consistent with variations in the C/N ratio. Therefore, we cannot relate changes in Hg concentration to the source of organic matter.

Comparison of Hg Accumulation in the Three Cores

The median Hg concentrations in the sediments of the Congo Basin (93.4 $\mu g\ kg^{-1}$) and Peru Margin (90.7 $\mu g\ kg^{-1}$) are similar. These concentrations are a factor of ∼2.5 times higher than the Hg concentrations in the Amazon Fan sediments (35.8 $\mu g\ kg^{-1}$). However, the highest Hg accumulation rate was found in the Peru Margin. The average Hg accumulation rate in the Peru Margin (∼178 $\mu g\ m^{-2}\ yr^{-1}$) is a factor of ∼4 and 39 times higher than that in the Congo Basin (46.7 $\mu g\ m^{-2}\ yr^{-1}$) and Amazon Fan (4.52 $\mu g\ m^{-2}\ yr^{-1}$), respectively.

The results of Hg analyses for our three studied cores show that median Hg concentrations were higher in the cores with higher organic carbon concentrations. The source of organic matter also affected the Hg concentration. In the Congo Basin and Peru Margin sediments, the higher Hg concentrations corresponded to lower C/N ratios and vice versa. Similar to what has been observed in sediments of the ocean with waters with high biological productivity (Zaferani et al., 2018), we suggest that Hg scavenging by marine-derived organic matter strongly increases Hg export from the water phase to the sediment. Among the three sites where we collected cores, the Peru Margin is a major upwelling

TABLE 3 | Factor loadings for the five significant components extracted by PCA from Amazon Fan sediment samples.

Variables	Components				
	1	2	3	4	5
Rb	**0.98**	0.05	0.11	0.08	0.00
Ca	**−0.97**	0.05	0.04	−0.05	0.15
Y	**0.97**	0.04	−0.09	−0.01	0.02
Pb	**0.97**	−0.02	0.01	0.05	0.06
Sr	**−0.95**	−0.07	0.06	−0.10	0.16
Zn	**0.90**	−0.05	0.29	0.08	0.10
Ti	**0.88**	0.39	−0.16	−0.08	−0.04
Al	**−0.85**	0.45	0.03	0.06	0.05
Fe	**0.83**	−0.08	0.27	0.08	0.26
Ni	**0.68**	−0.10	**0.61**	0.11	0.14
Hg	**0.58**	0.09	0.12	0.44	−0.35
K	0.11	**0.94**	0.00	−0.15	0.09
Si	−0.18	**0.89**	−0.21	−0.10	0.02
Cl	−0.57	**0.67**	−0.01	0.20	−0.06
S	0.25	**0.63**	0.00	0.09	−0.07
Mn	−0.28	0.00	**0.74**	−0.10	−0.01
Cu	0.28	−0.19	**0.73**	0.08	−0.04
C	−0.07	−0.05	−0.03	**0.87**	−0.03
N	0.08	−0.02	0.02	**0.85**	−0.02
Br	0.51	0.07	0.51	**0.54**	0.12
As	−0.29	0.04	0.35	0.09	**0.78**
Zr	0.33	−0.02	−0.29	−0.17	**0.76**
Eigenvalue	9.68	3.07	2.4	1.85	1.23
%Variance	44	14	11	8	6

Significant values are in bold.

site. Covariations of Hg with organic C and trace metals involved in biological cycling (e.g., Ni and Cu) (Böning et al., 2015) in Peru Margin sediments suggest that productivity is the major factor causing a high Hg accumulation rate. It has been shown that particles transfer as aggregates through Peruvian upwelled waters. The high Hg enrichment in Peru Margin sediments is caused by the scavenging of dissolved water-phase Hg by a large number of fast-sinking productivity-related particles. Hg removal from the water column by particulate matter would also likely decrease Hg re-evasion to the atmosphere, as previously assumed in model studies (Soerensen et al., 2014, 2016).

Considering that the lower Hg accumulation rates in the sediment cores were influenced by the world's largest rivers, i.e., the Congo Basin and Amazon Fan, we suggest that in the marine environment, scavenging and sedimentation of atmospheric-derived Hg by algal organic particles are of greater importance for Hg burial in sediment than Hg input from rivers. The Amazon River and Congo River are among the largest exporters of freshwater to marine waters globally and have very large catchments. These rivers, as tropical rivers, transport a very large amount of sediments, i.e., suspended solids, dissolved solutes, and organic matter. Based on the previous studies, that considered riverine Hg inputs as some of the largest sources of Hg to coastal oceans (Amos et al., 2014; Zhang et al., 2015), it was expected that these two rivers, with large catchments, high flow, and strong erosive power, would export large amounts of Hg to the ocean which are reflected by high Hg accumulation rates in river mouth sediments. However, none of the abovementioned characteristics led to higher Hg sedimentation than that in the upwelling system. One reason could be the evasion of Hg to the atmosphere. Most of riverine Hg can be subjected to evasion rather than being buried in sediments. This is while the scavenged Hg by productivity-related particles in the water column is buried more rapidly in sediments. The scavenging of Hg has an important control on the residence time of Hg waters (Tesán Onrubia et al., 2020). This phenomenon facilitates the downward flux of Hg to the seafloor which could be slow otherwise. Large river catchments also receive and store large amounts of Hg through atmosphere deposition which can be exported to the water. However, this Hg can be sequestered in soils and plant materials which further delays Hg export to the ocean. Nevertheless, we need to consider that the river mouth cores might suffer from the grain size separation which can result in under/overestimation of Hg concentrations and accumulation rates. Owing to the limited number and geographical scope of our studied cores, compared to the entire ocean, further investigation is needed to better understand our preliminary estimates.

CONCLUSION

We compared Hg accumulation in three marine sediment cores collected from fans of two large rivers with large terrestrial catchments and an upwelling area. Sediment Hg concentrations exhibited similar ranges at the locations where upwelling occurs (Peru Margin and Congo Basin) but were significantly lower in the Amazon River fan, where no upwelling occurs. Hg accumulation rates in Peru Margin sediments, where marine productivity and organic carbon concentrations are high, were a factor of ∼4 and 39 times higher than those in the Congo Basin and Amazon Fan, respectively. The PCA results of the geochemical data set reveal that Amazon Fan sediments are strongly influenced by the deposition of terrestrial material, which is of less importance in Congo Basin sediments and of minor importance in Peru Margin sediments. Accordingly, Hg export to sediments in upwelling areas largely surpasses that in fans of large rivers that drain large terrestrial catchments. The high Hg accumulation rates in the sediments in the upwelling area and the minor influence of terrestrial Hg fluxes there indicate that atmospheric-derived Hg in upwelling areas is effectively exported to the sediments through scavenging by organic particulates. Our results suggest that upwelling regions are of great importance in the marine Hg cycle for the sequestration of atmospheric-derived Hg and support previous assumptions that the removal of Hg from the water phase will reduce Hg re-evasion to the atmosphere. Our sediment core investigations, from locations influenced by the two largest rivers in the world in terms of freshwater discharge (Amazon River and Congo River),

further indicate that the influence of high productivity and related scavenging of Hg by sinking particles/organic matter even surpasses the influence of large river inputs, although more sediment studies are needed to confirm this conclusion. Biogeochemical processes that affect the final fate of riverine Hg in the ocean Hg could be different in different latitudes. More investigation is needed to better understand Hg behavior in these regions.

DATA AVAILABILITY STATEMENT

The original contributions presented in the study are included in the article/**Supplementary Material**, further inquiries can be directed to the corresponding author/s.

AUTHOR CONTRIBUTIONS

SZ carried out the analyses. HB supervised the findings of this work. Both authors wrote the manuscript.

FUNDING

This research was supported by Technische Universitaet Braunschweig.

ACKNOWLEDGMENTS

The authors would like to thank Golf Coast Repository and Bremen Core Repository for providing samples. The authors would also like to thank Petra Schmidt and Adelina Calean for their technical assistance. The authors acknowledge support by the Open Access Publication Funds of Technische Universität Braunschweig.

SUPPLEMENTARY MATERIAL

The Supplementary Material for this article can be found online at: https://www.frontiersin.org/articles/10.3389/fmars.2021.732720/full#supplementary-material

REFERENCES

Amos, H. M., Jacob, D. J., Kocman, D., Horowitz, H. M., Zhang, Y., Dutkiewicz, S., et al. (2014). Global biogeochemical implications of mercury discharges from rivers and sediment burial. *Environ. Sci. Technol.* 48, 9514–9522.

Amos, H. M., Jacob, D. J., Streets, D. G., and Sunderland, E. M. (2013). Legacy impacts of all-time anthropogenic emissions on the global mercury cycle. *Glob. Biogeochem. Cycles* 27, 410–421. doi: 10.1002/gbc.20040

Böning, P., Shaw, T., Pahnke, K., and Brumsack, H. J. (2015). Nickel as indicator of fresh organic matter in upwelling sediments. *Geochim. Cosmochim. Acta* 162, 99–108. doi: 10.1016/j.gca.2015.04.027

Bowman, K. L., Hammerschmidt, C. R., Lamborg, C. H., and Swarr, G. (2015). Mercury in the North Atlantic Ocean: The U.S. GEOTRACES zonal and meridional sections. *Deep. Res. Part II Top. Stud. Oceanogr.* 116, 251–261. doi: 10.1016/j.dsr2.2014.07.004

Caley, T., Malaizé, B., Zaragosi, S., Rossignol, L., Bourget, J., Eynaud, F., et al. (2011). New Arabian Sea records help decipher orbital timing of Indo-Asian monsoon. *Earth Planet. Sci. Lett.* 308, 433–444. doi: 10.1016/j.epsl.2011.06.019

Chavez, F. P., Bertrand, A., Guevara-Carrasco, R., Soler, P., and Csirke, J. (2008). The northern Humboldt Current System: Brief history, present status and a view towards the future. *Prog. Oceanogr.* 79, 95–105. doi: 10.1016/j.pocean.2008.10.012

Cheburkin, A. K., and Shotyk, W. (1996). An energy-dispersive miniprobe multielement analyzer (EMMA) for direct analysis of Pb and other trace elements in peats. *Fresenius. J. Anal. Chem.* 354, 688–691. doi: 10.1007/s0021663540688

Chester, R. (2003). "The transport of material to the oceans: relative flux magnitudes," in *Marine Geochemistry*, 2nd Edn, eds H. D. Schulz and M. Zabel (Oxford: Blackwell Science).

Cossa, D., Heimbu, L., Lannuzel, D., Rintoul, S. R., Butler, E. C. V., Bowie, A. R., et al. (2011). Mercury in the Southern Ocean. *Geochim. Cosmochim. Acta* 75, 4037–4052. doi: 10.1016/j.gca.2011.05.001

Cossa, D., Heimbürger, L. E., Pérez, F. F., García-Ibáñez, M. I., Sonke, J. E., Planquette, H., et al. (2018). Mercury distribution and transport in the North Atlantic Ocean along the GEOTRACES-GA01 transect. *Biogeosciences* 15, 2309–2323. doi: 10.5194/bg-15-2309-2018

Croudace, I. W., and Rothwell, R. G. (2015). *Micro-XRF Studies of Sediment Cores: Applications of a non-destructive tool for the environmental sciences*. Dordrecht: Springer, doi: 10.1007/978-94-017-9849-5

D'Croz, L., and O'Dea, A. (2007). Variability in upwelling along the Pacific shelf of Panama and implications for the distribution of nutrients and chlorophyll. *Estuar. Coast. Shelf Sci.* 73, 325–340. doi: 10.1016/j.ecss.2007.01.013

D'Hondt, S., Jørgensen, B., Miller, D., and Al, E. (2003). Site 1228. *Proc. Ocean Drill. Program Initial Rep.* 201, 77845–79547.

De Mendiola, B. R. (1981). Seasonal phytoplankton distribution along the Peruvian coast. *Coast. Upwell.* 1, 348–356. doi: 10.1029/co001p0348

DiTullio, G. R., Geesey, M. E., Maucher, J. M., Alm, M. B., Riseman, S. F., and Bruland, K. W. (2005). Influence of iron on algal community composition and physiological status in the Peru upwelling system. *Limnol. Oceanogr.* 50, 1887–1907. doi: 10.4319/lo.2005.50.6.1887

Driscoll, C. T., Mason, R. P., Chan, H. M., Jacob, D. J., and Pirrone, N. (2013). Mercury as a global pollutant: Sources, pathways, and effects. *Environ. Sci. Technol.* 47, 4967–4983. doi: 10.1021/es305071v

EPA (1998). *Mercury in solids and solutions by thermal decomposition, amalgamation, and atomic absorption spectropho-tometry*. Washington, DC: Environ. Prot. Agency.

Figueiredo, T. S., Albuquerque, A. L. S., Sanders, C. J., Cordeiro, L. G. M. S., and Silva-Filho, E. V. (2013). Mercury deposition during the previous century in an upwelling region; Cabo Frio, Brazil. *Mar. Pollut. Bull.* 76, 389–393. doi: 10.1016/j.marpolbul.2013.07.049

Fitzgerald, W. F., Gill, G. A., and Kim, J. P. (1984). An equatorial Pacific Ocean source of atmospheric mercury. *Science* 224, 597–599. doi: 10.1126/science.224.4649.597

Fitzgerald, W. F., Lamborg, C. H., and Hammerschmidt, C. R. (2007). Marine biogeochemical cycling of mercury. *Chem. Rev.* 107, 641–662. doi: 10.1021/cr050353m

Flood, R., Piper, D., Klaus, A., and Others, A. (1995). Site 941. *Proc. Ocean Drill. Program Initial Rep.* 155, 505–536.

Heimburger, L. E., Sonke, J. E., Cossa, D., Point, D., Lagane, C., Laffont, L., et al. (2015). Shallow methylmercury production in the marginal sea ice zone of the central Arctic Ocean. *Sci. Rep.* 5, 1–6. doi: 10.1038/srep10318

Horowitz, H. M., Jacob, D. J., Zhang, Y., DIbble, T. S., Slemr, F., Amos, H. M., et al. (2017). A new mechanism for atmospheric mercury redox chemistry: implications for the global mercury budget. *Atmos. Chem. Phys.* 17, 6353–6371. doi: 10.5194/acp-17-6353-2017

Jaisi, D. P., and Blake, R. E. (2010). Tracing sources and cycling of phosphorus in Peru Margin sediments using oxygen isotopes in authigenic and detrital

phosphates. *Geochim. Cosmochim. Acta* 74, 3199–3212. doi: 10.1016/j.gca.2010.02.030

Jensen, S., and Jernelöv, A. (1969). Biological methylation of mercury in aquatic organisms. *Nature* 223, 753–754.

Jiskra, M., Heimburger-Boavida, L.-E., Desgranges, M.-M., Petrova, M., Dufour, A., Ferreira-Araujo, B., et al. (2020). Mercury stable isotope composition of seawater suggests important net gaseous elemental mercury uptake. *EarthArXiv* [Preprint]. doi: 10.31223/osf.io/k6f8m

Keswani, S. R., Dunham, K. W., and Meyers, P. A. (1984). Organic geochemistry of late Cenozoic sediments from the subtropical South Atlantic Ocean. *Mar. Geol.* 61, 25–42. doi: 10.1016/0025-3227(84)90106-3

Kim, H., Soerensen, A. L., Hur, J., Heimbürger, L. E., Hahm, D., Rhee, T. S., et al. (2017). Methylmercury Mass Budgets and Distribution Characteristics in the Western Pacific Ocean. *Environ. Sci. Technol.* 51, 1186–1194. doi: 10.1021/acs.est.6b04238

Kim, J. P., and Fitzgerald, W. F. (1986). Sea-air partitioning of mercury in the equatorial Pacific Ocean. *Science* 231, 1131–1133.

Lamborg, C. H., Fitzgerald, W. F., O'Donnell, J., and Torgersen, T. (2002). A non-steady-state compartmental model of global-scale mercury biogeochemistry with interhemispheric atmospheric gradients. *Geochim. Cosmochim. Acta* 66, 1105–1118. doi: 10.1016/S0016-7037(01)00841-9

Lamborg, C., Bowman, K., Hammerschmidt, C., Gilmour, C., Munson, K., Selin, N., et al. (2014). Mercury in the Anthropocene Ocean. *Oceanography* 27, 76–87. doi: 10.5670/oceanog.2014.11

Lamborg, C. H., Hammerschmidt, C. R., Bowman, K. L., Swarr, G. J., Munson, K. M., Ohnemus, D. C., et al. (2014). A global ocean inventory of anthropogenic mercury based on water column measurements. *Nature* 512, 65–68. doi: 10.1038/nature13563

Le Faucheur, S., Campbell, P. G., Fortin, C., and Slaveykova, V. I. (2014). Interactions between mercury and phytoplankton: speciation, bioavailability, and internal handling. *Environ. Toxicol. Chem.* 33, 1211–1224. doi: 10.1002/etc.2424

Leri, A. C., Mayer, L. M., Thornton, K. R., Northrup, P. A., Dunigan, M. R., Ness, K. J., et al. (2015). A marine sink for chlorine in natural organic matter. *Nat. Geosci.* 8, 620–624. doi: 10.1038/ngeo2481

Mahaffey, K. R., Sunderland, E. M., Chan, H. M., Choi, A. L., Grandjean, P., Mariën, K., et al. (2011). Balancing the benefits of n-3 polyunsaturated fatty acids and the risks of methylmercury exposure from fish consumption. *Nutr. Rev.* 69, 493–508.

Mason, R. P., and Fitzgerald, W. F. (1993). The distribution and biogeochemical cycling of mercury in the equatorial Pacific Ocean. *Deep Sea Res. Part I Oceanogr. Res. Pap.* 40, 1897–1924. doi: 10.1016/0967-0637(93)90037-4

Mason, R. P., Choi, A. L., Fitzgerald, W. F., Hammerschmidt, Chad, R., Lamborg, C. H., et al. (2012). Mercury biogeochemical cycling in the ocean and policy implications. *Environ. Res.* 119, 101–117. doi: 10.1016/j.envres.2012.03.013

Mason, R. P., Fitzgerald, W. F., and Morel, F. M. (1994). The biogeochemical cycling of elemental mercury: anthropogenic influences. *Geochim. Cosmochim. Acta* 58, 3191–3198. doi: 10.1016/0016-7037(94)90046-9

Mason, R. P., Hammerschmidt, C. R., Lamborg, C. H., Bowman, K. L., Swarr, G. J., and Shelley, R. U. (2017). The air-sea exchange of mercury in the low latitude Pacific and Atlantic Oceans. *Deep. Res. Part I Oceanogr. Res. Pap.* 122, 17–28. doi: 10.1016/j.dsr.2017.01.015

Mason, R. P., Reinfelder, J. R., and Morel, F. M. (1996). Uptake, Toxicity, and Trophic Transfer of Mercury in a Coastal Diatom. *Environ. Sci. Technol.* 30, 1835–1845. doi: 10.1021/es950373d

Mason, R., and Sheu, G.-R. (2002). Role of the ocean in the global mercury cycle. *Glob. Biogeochem. Cycles* 16, 1–14. doi: 10.1029/2001GB001440

McKee, B. A., Aller, R. C., Allison, M. A., Bianchi, T. S., and Kineke, G. C. (2004). Transport and transformation of dissolved and particulate materials on continental margins influenced by major rivers: Benthic boundary layer and seabed processes. *Cont. Shelf Res.* 24, 899–926. doi: 10.1016/j.csr.2004.02.009

Morel, F. M., and Price, N. (2003). The biogeochemical cycles of trace metals in the oceans. *Science* 300, 944–947. doi: 10.1126/science.1083545

Munson, K. M., Lamborg, C. H., Swarr, G. J., and Saito, M. A. (2015). Mercury species concentrations and fluxes in the Central Tropical Pacific Ocean. *Glob. Biogeochem. Cycles* 29, 656–676.

O'Driscoll, N. J., Siciliano, S. D., Lean, D. R. S., and Amyot, M. (2006). Gross photoreduction kinetics of mercury in temperate freshwater lakes and rivers: Application to a general model of DGM dynamics. *Environ. Sci. Technol.* 40, 837–843. doi: 10.1021/es051062y

Outridge, P. M., Mason, R. P., Wang, F., Guerrero, S., and Heimbürger-Boavida, L. E. (2018). Updated global and oceanic mercury budgets for the United Nations Global Mercury Assessment 2018. *Environ. Sci. Technol.* 52, 11466–11477. doi: 10.1021/acs.est.8b01246

Premuzic, E. T., Benkovitz, C. M., Gaffney, J. S., and Walsh, J. J. (1982). The nature and distribution of organic matter in the surface sediments of world oceans and seas. *Org. Geochem.* 4, 63–77. doi: 10.1016/0146-6380(82)90009-2

Qureshi, A., O'Driscoll, N. J., Macleod, M., Neuhold, Y. M., and Hungerbühler, K. (2010). Photoreactions of mercury in surface ocean water: Gross reaction kinetics and possible pathways. *Environ. Sci. Technol.* 44, 644–649. doi: 10.1021/es9012728

Ren, J., Jiang, H., Seidenkrantz, M. S., and Kuijpers, A. (2009). A diatom-based reconstruction of Early Holocene hydrographic and climatic change in a southwest Greenland fjord. *Mar. Micropaleontol.* 70, 166–176. doi: 10.1016/j.marmicro.2008.12.003

Sanei, H., Outridge, P. M., Oguri, K., Stern, G. A., Thamdrup, B., Wenzhöfer, F., et al. (2021). High mercury accumulation in deep-ocean hadal sediments. *Sci. Rep.* 11, 1–8. doi: 10.1038/s41598-021-90459-1

Schartup, A. T., Balcom, P. H., Soerensen, A. L., Gosnell, K. J., Calder, R. S., Mason, R. P., et al. (2015). Freshwater discharges drive high levels of methylmercury in Arctic marine biota. *Proc. Natl. Acad. Sci. U S A.* 112, 11789–11794. doi: 10.1073/pnas.1505541112

Schartup, A. T., Qureshi, A., Dassuncao, C., Thackray, C. P., Harding, G., and Sunderland, E. M. (2018). A model for methylmercury uptake and trophic transfer by marine plankton. *Environ. Sci. Technol.* 52, 654–662. doi: 10.1021/acs.est.7b03821

Schartup, A. T., Thackray, C. P., Qureshi, A., Dassuncao, C., Gillespie, K., Hanke, A., et al. (2019). Climate change and overfishing increase neurotoxicant in marine predators. *Nature* 572, 648–650. doi: 10.1038/s41586-019-1468-9

Scheidegger, K. F., and Krissek, L. A. (1983). "Zooplankton and nekton: natural barriers to the seaward transport of suspended terrigenous particles off Peru," in *Coastal Upwelling Its Sediment Record*, eds E. Suess and J. Thiede (Berlin: Springer), doi: 10.1007/978-1-4615-6651-9_16

Selin, N. E. (2009). Global biogeochemical cycling of mercury: a review. *Annu. Rev. Environ. Resour.* 34, 43–63. doi: 10.1146/annurev.environ.051308.084314

Soerensen, A. L., Mason, R. P., Balcom, P. H., and Sunderland, E. M. (2013). Drivers of surface ocean mercury concentrations and air-sea exchange in the West Atlantic Ocean. *Environ. Sci. Technol.* 47, 7757–7765. doi: 10.1021/es401354q

Soerensen, A. L., Mason, R. P., Balcom, P. H., Jacob, D. J., Zhang, Y., Kuss, J., et al. (2014). Elemental mercury concentrations and fluxes in the tropical atmosphere and Ocean. *Environ. Sci. Technol.* 48, 11312–11319. doi: 10.1021/es503109p

Soerensen, A. L., Schartup, A. T., Gustafsson, E., Gustafsson, B. G., Undeman, E., and Bjoörn, E. (2016). Eutrophication increases phytoplankton methylmercury concentrations in a coastal sea - A Baltic sea case study. *Environ. Sci. Technol.* 50, 11787–11796. doi: 10.1021/acs.est.6b02717

Strode, S. A., Jaeglé, L., Selin, N. E., Jacob, D. J., Park, R. J., Yantosca, R. M., et al. (2007). Air-sea exchange in the global mercury cycle. *Global Biogeochem. Cycles* 21, 1–12. doi: 10.1029/2006GB002766

Suess, E., and von Huene, R. (1988). Ocean Drilling Program Leg 112, Peru continental margin: Part 2, sedimentary history and diagenesis in a coastal upwelling environment. *Geology* 16, 939–943. doi: 10.1130/0091-76131988016<0939:ODPLPC<2.3.CO;2

Sunderland, E. M., and Mason, R. P. (2007). Human impacts on open ocean mercury concentrations. *Global Biogeochem. Cycles* 21, 1–15. doi: 10.1029/2006GB002876

Tarazona, J., and Arntz, W. (2001). "The Peruvian Coastal Upwelling System," in *Coastal marine ecosystems of Latin America*, (Berlin: Springer), doi: 10.1007/978-3-662-04482-7_17

Tesán Onrubia, J. A., Petrova, M. V., Puigcorbé, V., Black, E. E., Valk, O., Dufour, A., et al. (2020). Mercury Export Flux in the Arctic Ocean Estimated from $^{234}Th/^{238}U$ Disequilibria. *ACS Earth Sp. Chem.* 4, 795–801. doi: 10.1021/acsearthspacechem.0c00055

Uliana, E., Lange, C. B., and Wefer, G. (2002). Evidence for Congo River freshwater load in Late Quaternary sediments of ODP site 1077 (5°S, 10°E). *Palaeogeogr. Palaeoclimatol. Palaeoecol.* 187, 137–150. doi: 10.1016/S0031-0182(02)00514-X

Wefer, G., Berger, W., Richter, C., and Al, E. (1998). Site 1076. *Proc. Ocean Drill. Program Initial Rep.* 175, 87–113.

Zaferani, S., Pérez-rodríguez, M., and Biester, H. (2018). Diatom ooze—A large marine mercury sink. *Science* 361, 797–800. doi: 10.1126/science.aat2735

Zhang, Y., Jacob, D. J., Dutkiewicz, S., Amos, H. M., Long, M. S., and Sunderland, E. M. (2015). Global Biogeochemical Cycles discharged to the global and Arctic oceans. *Glob. Biogeochem. Cycles* 29, 854–864. doi: 10.1002/2015GB005124. Received

Ziegler, M., Jilbert, T., De Lange, G. J., Lourens, L. J., and Reichart, G. J. (2008). Bromine counts from XRF scanning as an estimate of the marine organic carbon content of sediment cores. *Geochem. Geophys. Geosyst.* 9, 1–6. doi: 10.1029/2007GC001932

Ziegler, M., Lourens, L., Tuenter, E., and Reichart, G. (2009). Anomalously high Arabian Sea productivity conditions during MIS 13. *Clim. Past* 5, 1989–2018. doi: 10.5194/cpd-5-1989-2009

Conflict of Interest: The authors declare that the research was conducted in the absence of any commercial or financial relationships that could be construed as a potential conflict of interest.

Publisher's Note: All claims expressed in this article are solely those of the authors and do not necessarily represent those of their affiliated organizations, or those of the publisher, the editors and the reviewers. Any product that may be evaluated in this article, or claim that may be made by its manufacturer, is not guaranteed or endorsed by the publisher.